Current Reference Generation based on Next Generation Grid Code Requirements of Grid-Tied Converters during Asymmetrical Faults

Taul, Mads Graungaard; Wang, Xiongfei; Davari, Pooya; Blaabjerg, Frede

Published in:
IEEE Journal of Emerging and Selected Topics in Power Electronics

DOI (link to publication from Publisher):
10.1109/JESTPE.2019.2931726

Publication date:
2020

Document Version
Accepted author manuscript, peer reviewed version

Current Reference Generation based on Next Generation Grid Code Requirements of Grid-Tied Converters during Asymmetrical Faults

Mads Graungaard Taul, *Student Member, IEEE,* Xiongfei Wang, *Senior Member, IEEE,*
Pooya Davari, *Senior Member, IEEE,* Frede Blaabjerg, *Fellow, IEEE,*

***Abstract*—Increased penetration of converter-based power generation has enforced system operators to require ancillary services from distributed generation in order to support the grid and improve the power system stability and reliability. Recent and next generation of grid codes require asymmetrical current provision during unbalanced faults for optimal voltage support. To address this, based on the highly used flexible positive and negative-sequence control method for current reference generation, this paper presents a general current reference strategy for asymmetrical fault control where a direct and explicit method is proposed to calculate power references and controller gains while simultaneously complying with converter current limitation and fulfilling the next generation of grid code requirements. The proposed method is tested for three distinct asymmetrical grid faults considering the requirements for dynamic voltage support of the recently revised German grid code as well as the next-generation grid codes. It is shown that the proposed method can improve the fault ride-through performance during asymmetrical faults compared to conventional solutions and comply with modern grid code requirements in a general and flexible manner.**

***Index Terms*—Grid-Connection, Voltage-Source Converter, Asymmetrical Grid Fault, Current Reference Generation, Fault Ride-Through, Dynamic Voltage Support**

I. Introduction

TODAY, a high penetration of converter-based links are being assembled between Renewable Energy Sources (RES) and the external grid. These links are formed by interfaces of Voltage-Source Converters (VSCs), which entail that it is mostly the control strategy rather than topology and physical properties of the converter, which dominates the dynamic and static behavior, performance, and stability of modern power systems. This increased penetration of converter-based power generation has enforced Transmissions System Operators (TSOs) to require fault ride-through capability of installed converters in order to provide grid support during abnormal events. As a natural consequence of lightning, abnormal weather conditions, insulator wear-out, and human errors, grid faults do occur where Single Line-to-Ground (SLG) and Double Line-to-Ground (DLG) faults are the most common types of grid faults [1]. During an asymmetrical fault, the current reference strategy of a converter can be established in a numerous of different ways depending on converter and grid requirements.

Even though asymmetrical faults account for almost all grid faults, most grid codes do not state any directions and requirements regarding negative-sequence current injection during any type of fault [2], [3]. Consequently, Balanced Positive Sequence Control (BPSC) is a widely used strategy in industrial applications [4]. Besides BPSC, which only provides positive-sequence current injection, a large body of literature describes methods for unbalanced current provision during asymmetrical faults [5]–[13]. These all have different control objectives such as the quality of injected current, mitigation of dc-link voltage ripple, and achievement of constant instantaneous active or reactive power provision. Additionally, several reviews of different asymmetrical current generation strategies including BPSC, constant active power control, constant reactive power control and Flexible Positive and Negative Sequence Control (FPNSC) are given in [14]–[16]. Here, the FPNSC is stated as a general and flexible control structure, which can accommodate several different control objectives dependent on two independent controller gains. Due to this flexibility, this structure is being highly utilized [8], [10], [15], [17] together with different varieties of it [4], [11]. Common to all of these methods is that the injection of positive and negative-sequence currents during asymmetrical faults is usually considered only from the converter point of view.

Seen from the grid point of view, limited work has been done considering the needs of the power system including grid code requirements. To that end, if only positive-sequence current is injected during an asymmetrical fault, the voltage is boosted in non-faulty phases, which may result in phase over-voltages. Furthermore, without provision of negative-sequence current during asymmetrical faults, the difficulty of fault detection is highly increased for power system protection devices [18]. Therefore, seen from a grid-supporting point of view, negative-sequence reactive current injection should be supplied during asymmetrical faults [18], [19]. As shown in [20], dual-sequence current provision can support the grid by attenuating the negative-sequence voltage and boosting the positive-sequence voltage simultaneously. In the light of this, the recently revised German grid code VDE-AR-N 4120, which concerns installation of generators to the high-voltage network, actually includes requirements for negative-sequence

Mads Graungaard Taul, Xiongfei Wang, Pooya Davari, and Frede Blaabjerg are all with the Department of Energy Technology at Aalborg University, Denmark (email: mkg@et.aau.dk, xwa@et.aau.dk, pda@et.aau.dk, fbl@et.aau.dk).

This work was supported by the Reliable Power Electronic-Based Power System (REPEPS) project at the Department of Energy Technology, Aalborg University as a part of the Villum Investigator Program funded by the Villum Foundation.

current injection during asymmetrical faults [21]. To that end, requirements for negative-sequence current injection to installations in the medium-voltage network is recently issued in 2017 in VDE-AR-N 4110 [22]. For an open-access summary of the drafts, please refer to [23], [24]. Here, dynamic reactive current support is demanded in the positive and negative sequences to minimize surges in non-faulty phases and achieve what is referred to as optimum grid support during asymmetrical grid faults. Considering the latest revisions from VDE, the current reference generation is no longer a question whether to improve different circumstances seen from the converter point of view, but to a higher extent fixed by e.g. the TSO in order to provide grid-supporting functionalities. Consequently, present current reference strategies (e.g. FPNSC) need to be able to manage this. The term *next-generation grid codes* is used as it is expected that with an increased share of converter-interfaced renewables, that future grid codes, like for the revisions from VDE, will demand dual-sequence current provision during asymmetrical faults. In this manner, how to calculate the power references of FPNSC during an asymmetrical fault in compliance with recent grid codes still remains an open question. In addition to this, how to determine the flexible gains which control the ratio between positive and negative-sequence active and reactive power needs to be further investigated. In [4], [11], the selection of controller gains is mapped to reveal its influence on the active and reactive power oscillations but no considerations of grid codes and voltage support are included.

Several studies consider the injection of positive and negative-sequence reactive current during asymmetrical faults to support the grid voltage [25]–[28]. In [25], [26], only the positive-sequence reactive current is regulated to comply with grid codes whereas the negative sequence reactive current is selected to eliminate active power oscillations during the fault. In [27], a strategy is developed to avoid over-voltages and under-voltages based on grid voltage steady-state limits by injection of both positive and negative-sequence reactive current. A more recent publication from this group discusses an optimized control solution that either boosts the positive-sequence voltage, attenuates the negative-sequence voltage, or maximizes the difference between positive and negative-sequence magnitudes [28]. However, common to both studies is that the grid code requirements is only explicitly considered for the positive-sequence reactive current.

A few studies address the requirements for positive and negative-sequence current provision [2], [29], [30]. Here, a dual-sequence current provision strategy is proposed, but the method developed is not as flexible and general as FPNSC. Moreover, [2] does not include limitation of the converter current along with a description on how to distribute the active and reactive power when the converter currents are saturated. Further, in [29], the full converter capacity is not utilized. In [30], new curves for asymmetrical fault ride-through is proposed together with dynamic limits for the voltage parameters. Howbeit, this method proposes an improvement to existing grid code requirements and might, for that reason, not be the one to be considered for industrial applications that only consider currently applicable requirements. From this, in addition to the need for a direct method of calculating the necessary power references where the reactive power is prioritized, a direct method for calculating the controller gains of the FPNSC, taking into account converter current limitation as well as requirements for negative-sequence current provision in the modern and next-generation of grid codes is needed. Therefore, based on the FPNSC method, this paper presents a current reference generation strategy for asymmetrical faults where the power references and flexible controller gains can be explicitly derived while complying with converter current limitation and the next generation of grid code requirements. To accomplish this, the paper is structured as follows: Section II introduces the system of interest and presents the development of the FPNSC method. An analytical expression for the maximum converter current is derived in Section III. Section IV presents the proposed strategy which is validated and compared with three conventional solutions in Section V. Section VI includes the experimental verification of the proposed method. Finally, the paper is concluded in Section VII.

II. Flexible Positive Negative Sequence Control

In order to develop a control structure which can operate successfully during unbalanced faults, a synchronization unit capable of accurately extracting the positive and negative sequences of the grid voltage is needed. This can be done in several ways including a Dual Second-Order Generalized Integrator PLL (DSOGI-PLL) [31] or a Decoupled Double Synchronous-Reference Frame PLL (DDSRF-PLL) [32]. Alongside accurate tracking of the positive and negative-sequence components, the current controller needs to be able to regulate the negative-sequence current in addition to the positive sequence. This is normally done using Proportional-Resonant (PR) controllers in the stationary-reference frame or by implementing a dual-sequence SRF current controller consisting of four PI controllers, two for each sequence component, in the synchronous-reference frame. Besides these, the converter behavior is highly dependent on how the current reference is generated, which is the focus of this paper.

As described previously, since this paper aims to provide grid-supporting functionalities in conformity with modern grid codes, it is desired to employ a method where both positive and negative-sequence currents can be injected and controlled in a flexible manner. This includes injection of active power synchronized to the positive-sequence voltage, injection of capacitive reactive power synchronized to the positive-sequence voltage (positive-sequence support) and injection

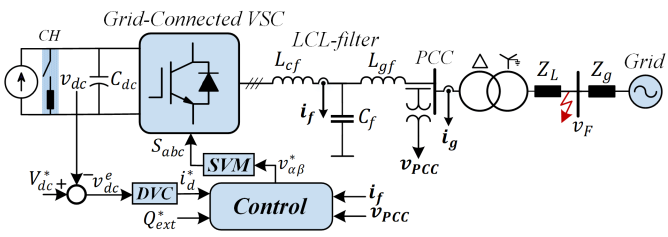

Fig. 1. Structure of distributed generator under study. The red arrow indicates the location of a grid fault. DVC: Direct Voltage Controller. SVM: Space Vector Modulation. CH: dc chopper circuit.

of inductive reactive power synchronized to the negative-sequence voltage (negative-sequence attenuation). To address this, the FPNSC framework is used in this work to generate the current references, which are to be calculated based on the proposed strategy. To that end, this paper employs a DSOGI-PLL for extracting the individual voltage sequences and PR controllers are used to regulate the positive and negative-sequence currents.

The distributed generator considered in this paper (visualized in Fig. 1) represents the grid-side converter of e.g. a wind turbine system or Photovoltaic (PV) system, which consists of a grid-connected converter interfaced with the Point of Common Coupling (PCC) through an LCL-filter. A Direct Voltage Controller (DVC) regulates the active power reference whereas the reactive power reference is obtained from a higher control layer. For a three-phase three-wire system as shown in Fig. 1, the voltages and currents can be fully described by the positive and negative-sequence components, [10], as

$$\mathbf{v} = \mathbf{v}^+ + \mathbf{v}^- \quad \text{and} \quad \mathbf{i} = \mathbf{i}^+ + \mathbf{i}^-. \tag{1}$$

Using the instantaneous power theory, the active and reactive power can be calculated as the dot product and cross product of the instantaneous voltages and currents respectively, as

$$p = \mathbf{v} \cdot \mathbf{i}, \quad q = \mathbf{v} \times \mathbf{i} = \mathbf{v}_\perp \cdot \mathbf{i} \tag{2}$$

where $\mathbf{v}_\perp$ is an orthogonal $90°$ leading version of the original positive-sequence voltage and a $90°$ lagging version in the case of an original negative-sequence voltages [33]. Expressed in the stationary-reference frame this can be written as

$$\mathbf{v}_{\perp\alpha\beta} = \begin{bmatrix} 0 & 1 \\ -1 & 0 \end{bmatrix} \mathbf{v}_{\alpha\beta}. \tag{3}$$

Inserting the positive and negative-sequence components in (2), the active and reactive powers can be expressed as

$$p = \underbrace{\mathbf{v}^+\mathbf{i}^+ + \mathbf{v}^-\mathbf{i}^-}_{\bar{P}} + \underbrace{\mathbf{v}^+\mathbf{i}^- + \mathbf{v}^-\mathbf{i}^+}_{\tilde{P}} \tag{4}$$

and

$$q = \underbrace{\mathbf{v}_\perp^+\mathbf{i}^+ + \mathbf{v}_\perp^-\mathbf{i}^-}_{\bar{Q}} + \underbrace{\mathbf{v}_\perp^+\mathbf{i}^- + \mathbf{v}_\perp^-\mathbf{i}^+}_{\tilde{Q}}. \tag{5}$$

The active and reactive powers consist of a constant term, originating from the dot product of voltage and current from the same sequence, and a second harmonic oscillatory term, originating from the dot product of voltage and current from different sequences. By isolating the injected currents and including flexible coefficients (k_1, k_2) designed to regulate the ratio between the positive and negative sequence for the active and reactive power respectively, the highly used FPNSC method is obtained as [8], [10], [16]

$$\mathbf{i_P}^* = P^* \left(\frac{k_1 \mathbf{v}^+}{|\mathbf{v}^+|^2} + \frac{(1-k_1)\mathbf{v}^-}{|\mathbf{v}^-|^2} \right), \tag{6}$$

$$\mathbf{i_Q}^* = Q^* \left(\frac{k_2 \mathbf{v}_\perp^+}{|\mathbf{v}^+|^2} + \frac{(1-k_2)\mathbf{v}_\perp^-}{|\mathbf{v}-|^2} \right). \tag{7}$$

Here $\mathbf{i_P}^*$ is the current vector contributing to active power whereas $\mathbf{i_Q}^*$ is the current vector contributing to reactive power. By expanding (6)-(7) into its $\alpha\beta$ components, the FPNSC method can be written as

$$\begin{aligned} i_\alpha^* = P^* \frac{2}{3} & \left(\frac{v_\alpha^+ k_1}{(v_\alpha^+)^2 + (v_\beta^+)^2} + \frac{v_\alpha^-(1-k_1)}{(v_\alpha^-)^2 + (v_\beta^-)^2} \right) \\ & + Q^* \frac{2}{3} \left(\frac{v_\beta^+ k_2}{(v_\alpha^+)^2 + (v_\beta^+)^2} + \frac{v_\beta^-(1-k_2)}{(v_\alpha^-)^2 + (v_\beta^-)^2} \right) \end{aligned} \tag{8}$$

$$\begin{aligned} i_\beta^* = P^* \frac{2}{3} & \left(\frac{v_\beta^+ k_1}{(v_\alpha^+)^2 + (v_\beta^+)^2} + \frac{v_\beta^-(1-k_1)}{(v_\alpha^-)^2 + (v_\beta^-)^2} \right) \\ & - Q^* \frac{2}{3} \left(\frac{v_\alpha^+ k_2}{(v_\alpha^+)^2 + (v_\beta^+)^2} + \frac{v_\alpha^-(1-k_2)}{(v_\alpha^-)^2 + (v_\beta^-)^2} \right) \end{aligned} \tag{9}$$

where P^* and Q^* are the references for the active and reactive power, respectively. The constant $2/3$ is included since a peak invariant Clarke transformation is used whereas for the instantaneous power theory, as discussed previously, a power invariant method was considered for simplified analysis. Since this method, depending on the selection of k_1 and k_2, might inject both positive and negative-sequence currents into the grid, it is needed to calculate the maximum current in each phase during an asymmetrical fault and limit it according to the maximum allowed value.

III. Derivation of Maximum Converter Currents

In order to limit the reference currents, an expression between the active and reactive power references, FPNSC coefficients (k_1 and k_2), and the corresponding converter current must be developed. Using the sequence components to represent the $\alpha\beta$-axis voltages as

$$v_\alpha^+ = V^+ \cos\big(\omega t + \phi^+\big), \quad v_\alpha^- = V^+ \cos\big(-\omega t + \phi^-\big), \tag{10}$$

$$v_\beta^+ = V^+ \sin\big(\omega t + \phi^+\big), \quad v_\beta^- = V^+ \sin\big(-\omega t + \phi^-\big), \tag{11}$$

where

$$V^+ = \sqrt{(v_\alpha^+)^2 + (v_\beta^+)^2}, \quad \phi^+ = \tan^{-1}\left(\frac{v_\beta^+}{v_\alpha^+}\right) - \omega t, \tag{12}$$

$$V^- = \sqrt{(v_\alpha^-)^2 + (v_\beta^-)^2}, \quad \phi^- = \tan^{-1}\left(\frac{v_\beta^-}{v_\alpha^-}\right) + \omega t. \tag{13}$$

and adopting the definitions from [8]

$$I_p^+ = \frac{2k_1 P^*}{3V^+}, \qquad I_p^- = \frac{2(1-k_1)P^*}{3V^-}, \tag{14}$$

$$I_q^+ = \frac{2k_2 Q^*}{3V^+}, \qquad I_q^- = \frac{2(1-k_2)Q^*}{3V^-}, \tag{15}$$

the current references presented in (8)-(9) can be written as

$$i_\alpha^* = I^+ \cos\big(\omega t + \phi^+ - \theta_p\big) + I^- \cos\big(\omega t - \phi^- + \theta_n\big), \tag{16}$$

$$i_\beta^* = I^+ \sin\big(\omega t + \phi^+ - \theta_p\big) - I^- \sin\big(\omega t - \phi^- + \theta_n\big), \tag{17}$$

where

$$I^+ = \sqrt{(I_p^+)^2 + (I_q^+)^2}, \qquad \theta_p = \tan^{-1}\left(\frac{I_q^+}{I_p^+}\right), \tag{18}$$

$$I^- = \sqrt{(I_p^-)^2 + (I_q^-)^2}, \qquad \theta_n = \tan^{-1}\left(\frac{I_q^-}{I_p^-}\right). \tag{19}$$

The positive-sequence and negative-sequence currents in (16)-(17) are shown in Fig. 2 where the addition of the positive and negative sequences form the resulting asymmetrical current, depicted as the elliptical loci in the stationary-reference frame. The goal is to derive an expression for the maximum value of the projection of the elliptical current to the *abc*-axes, which is shown as $(\hat{I}_a, \hat{I}_b, \hat{I}_c)$ in Fig. 2. Using the inverse Clarke transformation to derive the expression for the three-phase currents, this maximum projection can be calculated. This is expressed as

$$\mathbf{i}^*_{\mathbf{abc}} = \cos(\gamma) i^*_\alpha - \sin(\gamma) i^*_\beta, \tag{20}$$

where

$$\gamma = \begin{cases} 0 & \text{for phase-a,} \\ -2\pi/3 & \text{for phase-b,} \\ +2\pi/3 & \text{for phase-c.} \end{cases} \tag{21}$$

By expanding the trigonometric functions and using vector projections, e.g. $I^+\cos(\phi^+ - \theta_p) = I_p^+\cos(\phi^+) + I_q^+\sin(\phi^+)$, the phase currents can be expressed as

$$\mathbf{i}^*_{\mathbf{abc}} = \lambda_1 \cos(\omega t) + \lambda_2 \sin(\omega t) \tag{22}$$

where

$$\begin{aligned} \lambda_1 = &\left[I^+\cos\left(\phi^+ - \theta_p\right) + I^-\cos\left(\phi^- + \theta_n\right)\right]\cos(\gamma) \\ &- \left[I^+\sin\left(\phi^+ - \theta_p\right) - I^-\sin\left(\phi^- + \theta_n\right)\right]\sin(\gamma), \end{aligned} \tag{23}$$

$$\begin{aligned} \lambda_2 = &\left[-I^+\sin\left(\phi^+ - \theta_p\right) - I^-\sin\left(\phi^- + \theta_n\right)\right]\cos(\gamma) \\ &- \left[I^+\cos\left(\phi^+ - \theta_p\right) - I^-\cos\left(\phi^- + \theta_n\right)\right]\sin(\gamma). \end{aligned} \tag{24}$$

Finally, the magnitude of the phase current can be found as

$$\hat{I} = \sqrt{\lambda_1^2 + \lambda_2^2} \tag{25}$$

which by simplification and by combining trigonometric functions can be written as

$$\hat{I} = \sqrt{(I^+)^2 + (I^-)^2 + 2I^+I^-\cos(2\gamma + \delta - \theta_n - \theta_p)}, \tag{26}$$

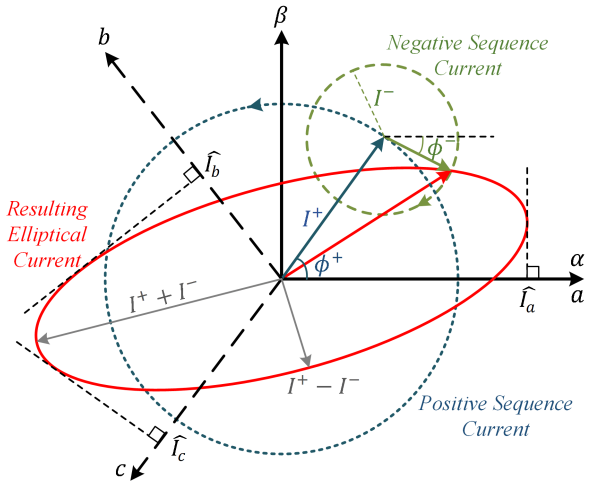

Fig. 2. Positive and negative-sequence currents, which form the elliptical current reference in the stationary-reference frame [9]. The maximum phase values are depicted as projections from the loci of the ellipse to the *abc*-axes.

where $\delta = \phi^+ - \phi^-$. This expression for the peak value of the phase currents is to be used subsequently when calculating the power references of the proposed strategy.

IV. Proposed Grid Code-based Current Reference Generation

This section presents the proposed strategy for generating the asymmetrical current references. First, the grid code requirements of interest are described and the associated reactive power reference needed for compliance is identified. Then, by using the developed expression for the peak value of the phase currents, the remaining capacity for active power provision is calculated such that the full converter capacity is utilized. Finally, the proposed strategy is described in a step-by-step manner in order to ease the understanding and the practical implementation of the method.

During a fault event, the requirements for the "stay-connected" duration vary depending on whether the generator considered is installed in the high-voltage or medium-voltage network and whether the fault is a three-phase or two-phase fault. The low-voltage ride-through requirements are shown in Fig. 3 for both grid codes considering negative-sequence current provision [21], [22]. It is evident that more strict performance is required by two-phase faults and for generators installed in the high-voltage network (VDE-AR-N 4120). In addition to the demand to stay connected, the installed generators should inject positive and negative-sequence reactive current proportional to the change in positive and negative-sequence voltage within 30 ms from fault detection. This is expressed as

$$\Delta i_Q^{+,-} = k^{+,-} \cdot \Delta v^{+,-} \tag{27}$$

where $v^+ = \frac{V^+ - V_{pf}}{V_N}$, $v^- = V^-/V_N$, V_{pf} is the mean value of the pre-fault network voltage measured over 50 fundamental cycles, and V_N is the nominal voltage. The proportionality

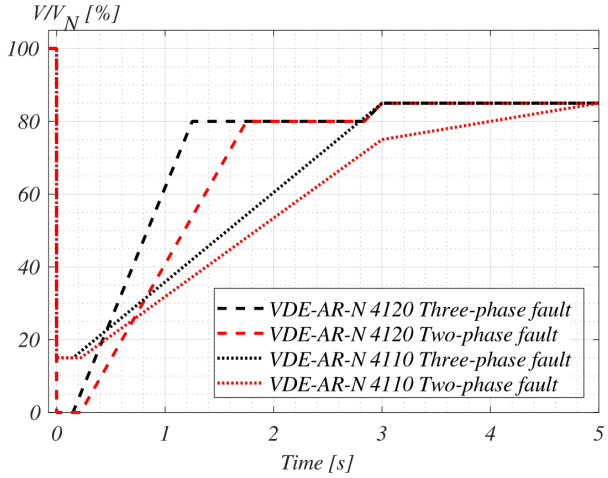

Fig. 3. Low-voltage ride-through requirements for both high-voltage (4120) and medium-voltage (4110) generators where voltage vs time profile for stay connected requirements is depicted. V_N is the nominal line-to-line voltage and V represents the smallest of the three line-to-line voltages during the fault. Black color represents the three-phase faults and the red color represents the two-phase faults.

factor should be set to two if not otherwise specified, but must be in the range $2 \leq k^{+,-} \leq 6$. With an expression for calculating the peak value of each individual phase current at hand (26), the selection of active and reactive power references can be described by taking into account the converter current constraint. As can be seen from (8) and (9), the α- and the β-axis each consists of two terms. One term defined by k_1, which distribute the active power reference into its positive and negative sequence components, and another term defined by k_2, which distribute the reactive power reference into its positive and negative sequence components. Using this, one may write the reactive power reference as the sum of its sequence components as

$$Q^* = Q^+ + Q^- \tag{28}$$

where each component must be defined as

$$Q^+ = Q^* k_2, \quad Q^- = Q^*(1 - k_2). \tag{29}$$

Previously, this relation was set based on some predefined ratio of the share of reactive power between the positive and negative sequence. Seen from the grid point of view, it might not be advantageous to select a constant value for k_2 but instead adaptively change it depending on the unbalance of the grid voltages. Considering that when a fault occurs, the maximum obtainable reactive power will be the power achieved if the full current capability is assigned to reactive current injection. To that end, the reactive current reference based on the grid code can be expressed as the positive and negative-sequence reactive power by

$$Q^+ = \begin{cases} 0 & \text{if } V^+ > 0.9, \\ k^+ Q_{max}(1 - V^+) & \text{if } 1 - 1/k^+ < V^+ < 0.9, \\ Q_{max} & \text{otherwise.} \end{cases} \tag{30}$$

and

$$Q^- = \begin{cases} 0 & \text{if } V^- < 0.1, \\ k^- Q_{max} V^- & \text{if } 0.1 < V^- < 1/k^-, \\ Q_{max} & \text{otherwise.} \end{cases} \tag{31}$$

The reactive power reference can then be expressed as

$$Q^* = Q^+ + Q^- = Q_{max}(k^+(1 - V^+) + k^- V^-) \tag{32}$$

and k_2 can then be calculated as

$$k_2 = \frac{Q^+}{Q^*} = \frac{k^+(1 - V^+)}{k^+(1 - V^+) + k^- V^-}. \tag{33}$$

From this, the reactive power is now divided between the positive and negative sequence depending on the voltage unbalance factor, rather than a predefined value with the purpose of suppressing power oscillating terms. For instance, if a symmetrical fault appears, no negative-sequence voltage will be present and $k_2 = 1$, meaning that only the drop in positive-sequence voltage will be considered. However, as the negative-sequence component of the grid voltage increases, k_2 will tend to zero meaning that more and more efforts will be devoted to attenuate the negative-sequence component rather than boosting the positive-sequence component.

As can be seen from (32), Q_{max} needs to be calculated in order to obtain the reactive power reference. As carefully proven in the Appendix, by expanding (26), the maximum phase current can be expressed as a function of the active and reactive power references together with the control coefficients (k_1, k_2) as shown in (34). Since the reactive power is prioritized over active power during a fault, Q_{max} is calculated for $P = 0$. Note that for severe conditions where the full converter capacity is assigned to reactive power, the maximum power point tracker in the case of PV applications or the pitch angle control in the case of wind turbine applications aim to reduce the harvested active power. In addition to this, a dc chopper is used to dissipate accumulation of energy on the dc-link capacitor to avoid destructive over-voltages.

Using the expression for the maximum phase current during the fault in (34), setting the active power reference to zero and solving for the reactive power reference, the maximum achievable value of reactive power without exceeding the phase current limitation is obtained as shown in (35). It should be noted that Q_{max} is the numerically smallest solution of Q calculated for the three values of γ. When Q_{max} is calculated, Q^+ and Q^- are calculated based on k^+ and k^- together with the amplitude of the positive and negative-sequence voltage components. Then, when Q^+ and Q^- have been calculated (inserted as $Q^* = Q^+ + Q^-$ in (34)), the remaining active power capacity is found by solving for the active power in

$$0 = aP_r^{*2} + bP_r^* + c - I_{lim}^2. \tag{36}$$

The workable solution for this is

$$P_r^* = \min\left(\frac{-b + \sqrt{-4a(c - I_{lim}^2) + b^2}}{2a}\right) \tag{37}$$

where the numerically smallest value of the solutions for γ is selected. The expressions for the coefficients of the second-order equation are visualized in (34). The calculated value of P_r^* is now compared to what is commanded by the dc-link voltage controller or any external active power reference to either safely send through the just calculated active power reference or require active power curtailment by reducing the reference in order to avoid destructive converter over-currents.

Ultimately, this strategy has the ability to adopt the widely used FPNSC method where the power references and the flexible gain selection of k_2 are uniquely determined in terms of recent grid code requirements, all while the converter currents are limited to its maximum allowed value. This method, therefore, assists in resolving several limitations from state-of-the-art literature. At first, by using the FPNSC, the power references are directly specified and do not take the form of unknown or assumed known. Secondly, the selection of k_1 and k_2 in the FPNSC method is now explicitly formulated based on the grid code requirements as opposed to being selected based on a desired power fluctuation profile. Accordingly, the advantages of employing the proposed strategy are:

- Explicit design of k_1, k_2, P^*, and Q^* under fault conditions in accordance with modern grid code requirements.
- Full utilization of the converter capacity.

$$\hat{I}^2 = (P^*)^2 \underbrace{\frac{4}{9}\left(\frac{k_1^2(V^-)^2 + (1-k_1)^2(V^+)^2 + 2k_1(1-k_1)\cos(2\gamma+\delta)V^+V^-}{(V^+)^2(V^-)^2}\right)}_{a} \underbrace{-\frac{4}{9}Q^*\left(\frac{2V^+V^-\sin(2\gamma+\delta)(k_1+k_2-2k_1k_2)}{(V^+)^2(V^-)^2}\right)}_{b} P^* + \underbrace{\frac{4}{9}(Q^*)^2\left(\frac{k_2^2(V^-)^2 + (1-k_2)^2(V^+)^2 - 2k_2(1-k_2)\cos(2\gamma+\delta)V^+V^-}{(V^+)^2(V^-)^2}\right)}_{c} \tag{34}$$

$$Q_{max} = \min\left(\frac{3}{2}\sqrt{\frac{I_{lim}^2(V^+)^2(V^-)^2}{k_2^2(V^-)^2 + (1-k_2)^2(V^+)^2 - 2k_2(1-k_2)\cos(2\gamma+\delta)V^+V^-}}\right) \tag{35}$$

- Improved voltage unbalance factor.
- Avoiding over-voltages at the PCC.

The proposed current reference generation strategy for asymmetrical fault ride-through is clearly summarized below in a step-by-step fashion:

① Identify k^+, k^- from the grid code, and specify I_{lim}.

② Calculate V^+, V^-, δ, k_2, and set $k_1 = 1$.
If $k^- = 0$, then set $k_2 = 0$ to avoid k_2 being undefined due to division by zero. Else if $V^- < 0.1$ pu then set $k_2 = 1$.

③ Calculate Q_{max} using (35). Note that if the denominator in the $\sqrt{\ }$ function is not strictly positive then set $Q_{max} = 0$. If $k_2 = 1$ then $Q_{max} = \frac{3}{2}I_{lim}V^+$, to also take symmetrical faults into account.

④ Calculate the required reactive power reference based on the grid code using (30), (31), and include the external reference such that $Q^* = Q^+ + Q^- + Q^*_{ext}$. Note that if $Q^* > Q_{max}$, then set $Q^* = Q_{max}$.

⑤ Calculate the remaining capacity for active power provision. Insert Q^* in (37) and solve for the lowest remaining capacity for active power P_r^* for the three values of γ. Note that, if $-4a(c - I_{lim}^2) + b^2 < 0$, then set $P_r^* = 0$.

⑥ Limit or pass the active power reference, which is calculated from the active current reference from the dc-link voltage controller (DVC) as

$$P^* = \frac{3}{2}i_d V^+. \tag{38}$$

Modify the active power reference if needed:

$$P^* = \begin{cases} P^* & \text{if } P_r^* > P^*, \\ 0 & \text{if } P_r^* \leq 0, \\ P_r^* & \text{otherwise.} \end{cases} \tag{39}$$

The control diagram of the proposed strategy including sequence extraction, the FPNSC method, current controller, and outer dc-link voltage controller is shown in Fig. 4.

a) Remarks: In the case that the current controller is implemented into two synchronous-reference frames, one for the each phase sequence, the current references in the stationary coordinates, as shown in (8)-(9), are simply transformed into dq-coordinates using the positive and negative sequence phase angles detected using the sequence extractor, here the DSOGI-PLL.

Besides this, with the presented method, it is needed to calculate the active and reactive power references alongside k_1, k_2 to fulfill the grid code requirements and safely limit the converter currents. From (27), one could instead directly use the expressions for the positive and negative sequence reactive current references without having to consider any power references. Since the components in (27) are dc values in steady-state, one could implement these current references directly in the dq-rotating frame. Considering this and $Q^*_{ext} = 0$, the dq-current references for both sequences may be calculated as

$$i_d^{+*} = f(v_{dc}, I_{lim}, i_q^{+-*}), \quad i_q^{+*} = -k^+\Delta v^+$$
$$i_d^{-*} = 0, \qquad i_q^{-*} = k^-\Delta v^-,$$

where i_d^{+*} needs to be calculated based on the needed active power from the dc-link controller while limiting the converter current and prioritizing reactive current injection. Even though this implementation is indeed possible and its derivation may be simplified, it may impair the controller computational efficiency. At first, two synchronous-references frames must be used, each containing two PI controllers. Secondly, a decoupling network should be included to eliminate second-order harmonic oscillations in the measurements, and four additional Park transformations are required for the calculation, which significantly increases the computational burden. In addition, the active and reactive power references are calculated in this work as it is beneficial to develop a method which can be directly applied to already existing solutions, e.g. FPNSC. In this way, the user can easily switch between different control objectives including the proposed method by only

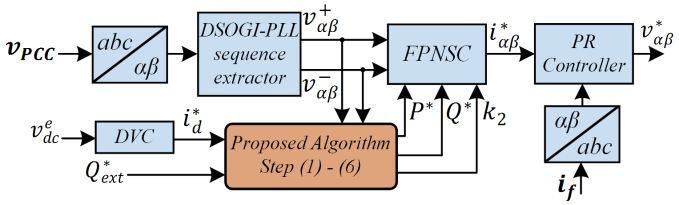

Fig. 4. Control diagram of proposed method including DSOGI-PLL for sequence extraction, FPNSC for generation of the current references and an inner current controller which provides the voltage reference for the VSC.

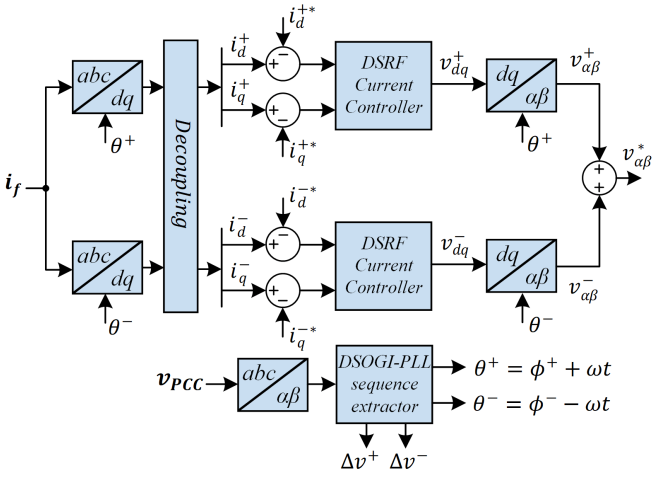

Fig. 5. Control block diagram of DDSRF current controller, which can be used to implement the control strategy in the synchronous-reference frame.

modifying k_1 and k_2. Nevertheless, if one desires to implement the current references directly in the synchronous-reference frame, this could be done using a DDSRF current controller as depicted in Fig. 5.

Lastly, it was mentioned in the introduction that the dynamics of the power system will be mostly dominated by the converter control rather than the topology. However, it should be noted as it is disclosed in [34], that a Modular Multilevel Converter (MMC) will observe limitations in the operating range during asymmetrical conditions due to its circuit topology. Here, some amount of zero-sequence provision needs to be provided to guarantee the balancing of the cell capacitors. To that end, for a condition where the unbalance factor approaches one, the requirements for zero-sequence provision approaches infinity. This is carefully mapped in [34] and should be addressed if an MMC topology is considered for the strategy presented in this work.

V. Validation and Comparison of Proposed Strategy

In this section, the proposed current reference generation strategy is tested during three asymmetrical grid faults and compared to three different design strategies using the FPNSC method. A simulation model is developed in MATLABs Simulink using PLECS blockset and the main parameters of the system in Fig. 1 are shown in Table I. The settling times of the DSOGI-PLL and the current controller are 20 ms and 10 ms, respectively. As evident from Table I, the converter current is constrained to 1.2 pu during the fault instead of the nominal current. Considering the short duration of the fault, then in practice, the power switches are typically capable of withstanding temporary higher currents [29], [35]. To take into account the coupling between sequences during the fault, a Delta-wye (Dy) grounded transformer is included, which can interact with the ground and the interconnected sequences at the fault location. Thus, the over-voltages experienced in a real application might not be recognized if the fault is simply emulated by controlling each grid phase voltage independently.

TABLE I
MAIN PARAMETERS OF THE SYSTEM IN FIG. 1.

Symbol	Description	Physical Value
S_b	Rated power	7.5 kVA
V_N	Nominal grid voltage	400 V
f_n	Nominal frequency	50 Hz
V_{dc}^*	dc-link voltage reference	730 V
Q_{ext}^*	External reactive power reference	0
C_{dc}	dc-link capacitance	0.5 mF
L_{cf}	Converter-side inductor	0.071 pu
L_{gf}	Grid-side inductor	0.043 pu
C_f	Filter capacitor	0.068 pu
f_{sw}	Switching frequency	10 kHz
f_s	Sampling frequency	10 kHz
Z_L	Line reactance	0.1 pu
Z_g	Grid impedance	0.1 pu
SCR	Short-circuit ratio	5
k^+, k^-	Grid code proportionality constants	2
I_{lim}	Maximum temporary converter current	1.2 pu
$K_{p,ic}$	Proportional gain PR controller	12
$K_{r,ic}$	Resonant gain of PR controller	2000

In that case, a set of voltages can be constructed and the response by the converter can be identified, but how the converter control is influencing the voltages in a realistic system cannot be accurately determined since the coupling between the phases is neglected.

Three fault types are considered: a single line-to-ground, a double line-to-ground, and a line-to-line fault. All faults are considered solid (zero fault impedance) and the performance of the proposed method is compared to three different usages of the FPNSC method: BPSC, constant active power control, and constant reactive power control.

At first, a comparison to the conventionally used BPSC is conducted. For the BPSC, the parameters in the FPNSC are selected as $k_1 = 1$ and $k_2 = 1$. For the second comparison, the gain parameters for the FPNSC method are selected as

$$k_1 = \frac{(V^+)^2}{(V^+)^2 - (V^-)^2}, \qquad k_2 = \frac{(V^+)^2}{(V^+)^2 + (V^-)^2} \tag{40}$$

which aim to accomplish constant instantaneous active power injection. The last comparison is between the proposed strategy and the constant instantaneous reactive power strategy. For this case, k_1 and k_2 are simply interchanged from what is shown in (40) [16]. For the BPSC, constant active power, and constant reactive power strategies, reactive power support is solely based on the positive-sequence requirements of the grid code with $k^+ = 2$. When the enforced reactive power has been calculated, the remaining capacity is allocated to active power injection with the restriction that the magnitude of the injected currents should remain less than I_{lim}. For all the simulated cases, if the remaining capacity for active power is lower than the feed-in dc-side power, then the dc-chopper circuit is activated to dissipate any accumulation of energy.

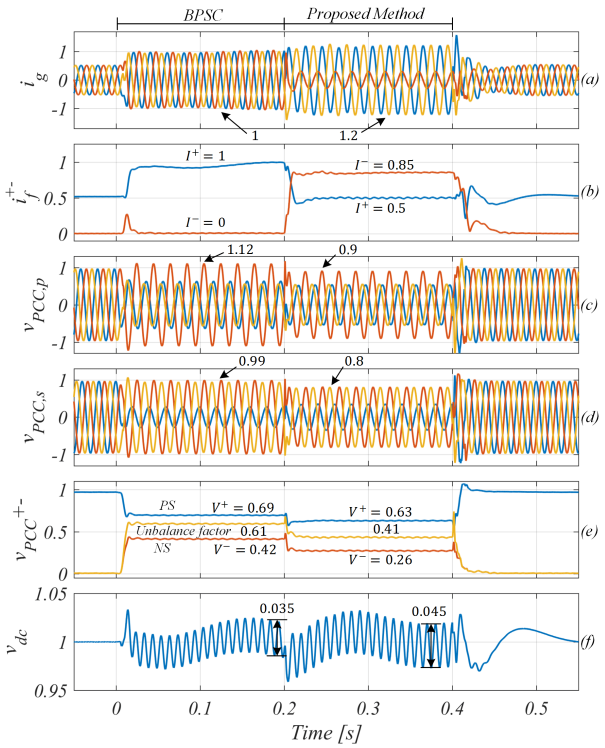

Fig. 6. Simulation results for a single line-to-ground solid fault for FPNSC using the BPSC design method and the proposed method.

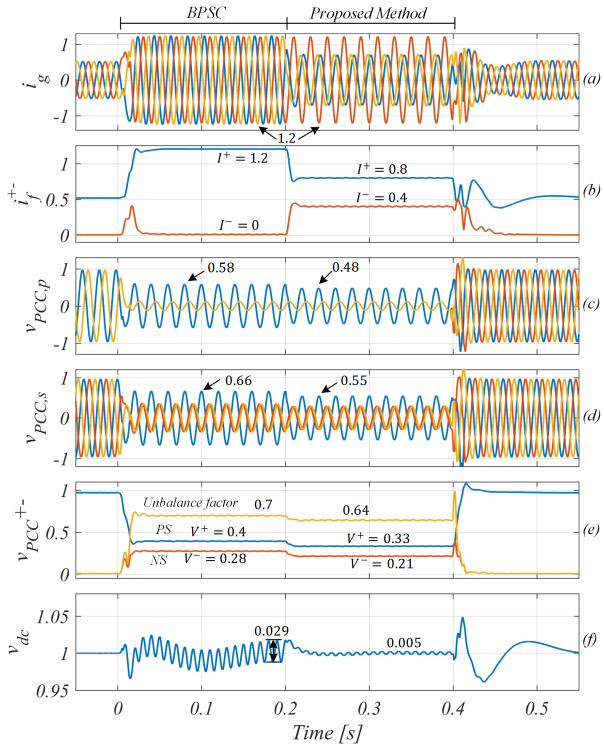

Fig. 7. Simulation results for a double line-to-ground solid fault for FPNSC using the BPSC design method and the proposed method.

A. Comparison to BPSC

The comparison to the BPSC method is presented in Fig. 6, Fig. 7, and Fig. 8 respectively. Each figure consists of six sub-figures (a)-(f) where (a) is the three-phase grid current, (b) is the positive and negative sequences of the converter current, (c) is the three-phase voltages at the primary-side of the Dy transformer, (d) is the three-phase voltages at the secondary-side of the Dy transformer, (e) is the positive sequence, negative sequence, and Voltage Unbalance Factor (VUF) (V^-/V^+) of the primary-side PCC voltage, and (f) is the voltage at the dc-link capacitor. All values are given in per-unit. As it can be seen in all three cases, the proposed method, which complies with the next generation of grid codes for negative-sequence reactive current provision, results in a lower voltage unbalance factor at the PCC. To that end, the peak-to-peak dc-link ripple is reduced for the line-to-line (Fig. 8) and the double line-to-ground faults (Fig. 7). Yet, the dc-link ripple is increased for the SLG fault. This occurs since the proposed strategy does not concentrate on the dc-link ripple but only on the positive and negative sequence requirements stated by the grid code.

From Fig. 6, it can be noticed that since only positive sequence support is considered for the BPSC, the full capacity of the converter is not being utilized, even though the active power from the dc-side is being transferred as well. Besides this, it can be seen from the SLG fault (Fig. 6) and the line-to-line fault (Fig. 8), that without provision of negative-sequence reactive current (BPSC), over-voltages occur in one or more of the PCC phase voltages. From Fig. 6, it can be seen that an over-voltage at 1.12 pu is present at the primary side of the

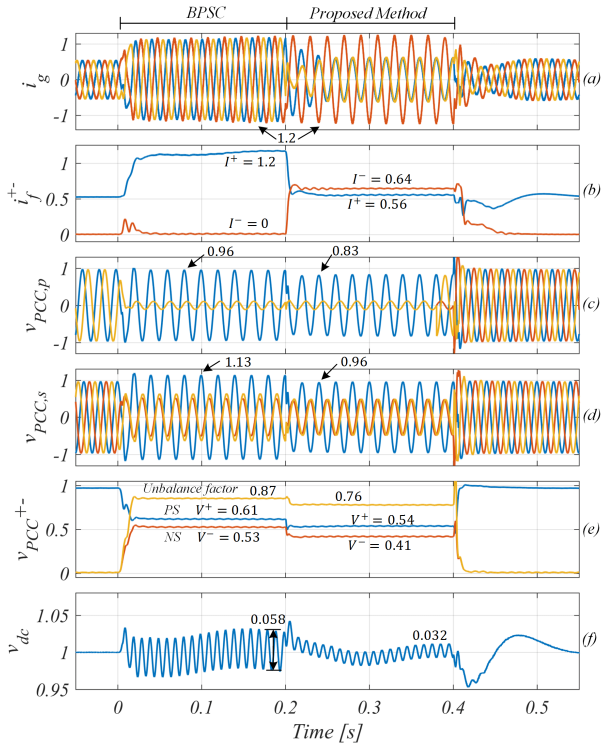

Fig. 8. Simulation results for a line-to-line solid fault for FPNSC using the BPSC design method and the proposed method.

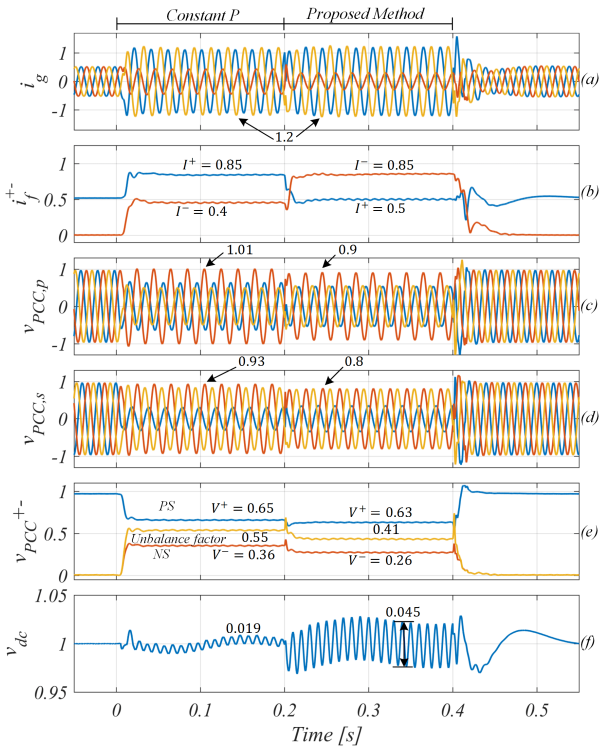

Fig. 9. Simulation results for a single line-to-ground solid fault for constant active power method and the proposed method.

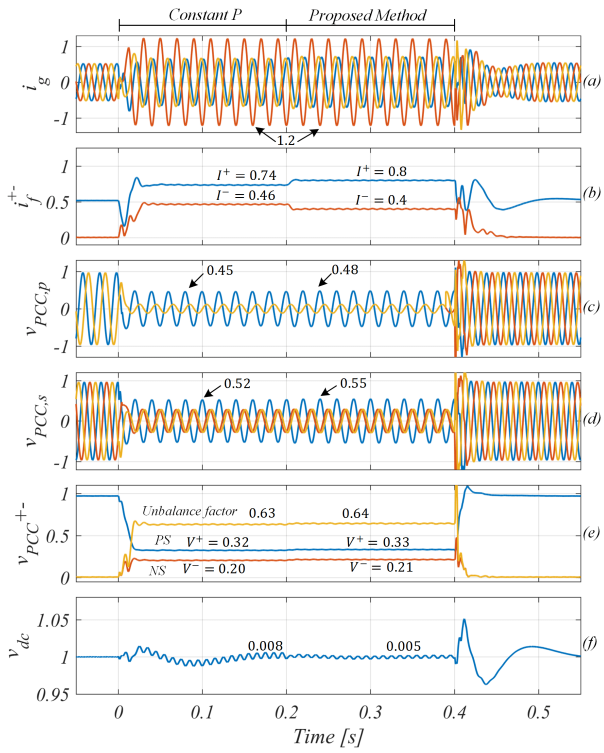

Fig. 10. Simulation results for a double line-to-ground solid fault for FPNSC using the constant active power design method and the proposed method.

Dy transformer. The opposite phenomenon is evident from the line-to-line fault in Fig. 8 where the PCC over-voltage is occurring at the secondary side rather than the primary side. Here the over-voltage at the secondary side is 1.13 pu with BPSC, where it is reduced to 0.96 pu using the proposed method as inductive reactive current is provided for negative-sequence attenuation.

B. Comparison to Constant Active Power Strategy

The results for the three considered fault types where the FPNSC method is designed to accomplish constant active power injection are shown in Fig. 9, Fig. 10, and Fig. 11. As the active power injection for this method is constant, a low dc-link ripple is evident from the results during all three fault types. As the FPNSC using the constant active power strategy only aims to inject positive sequence reactive current according to conventional grid codes, it can be seen that the positive sequence current injection is dominant using this strategy. Yet, the VUF is significantly lower when using the proposed method, which includes the negative sequence attenuation. For the DLG and line-to-line fault, these are both so severe that the full current capacity of the converter is being prioritized for voltage support. As can be seen from Fig. 10 and Fig. 11, the difference between constant active power injection and the proposed strategy is small even though the unbalance factor is improved using the proposed strategy for the line-to-line fault. This similarity between these two methods occurs since with a low-voltage fault, the full current capacity is being allocated to reactive power injection, meaning that the requested active power is reduced to zero. Therefore, the large

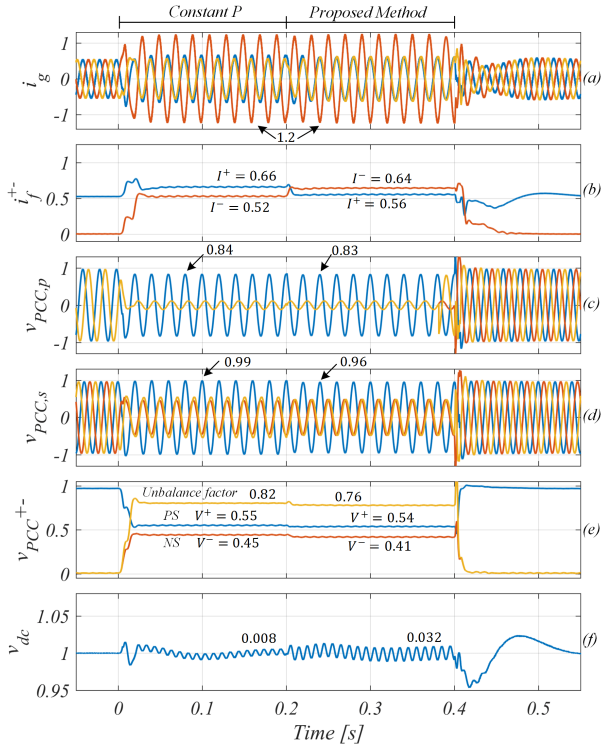

Fig. 11. Simulation results for a line-to-line solid fault for FPNSC using the constant active power design method and the proposed method.

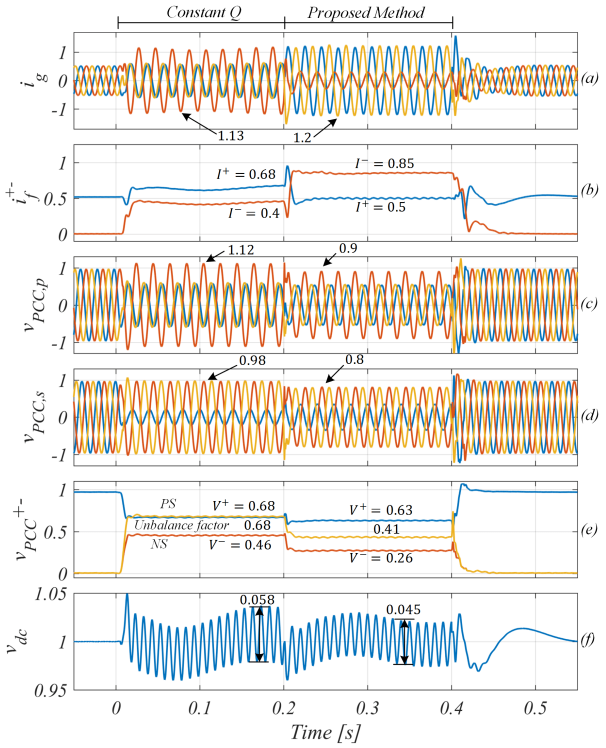

Fig. 12. Simulation results for a single line-to-ground solid fault for FPNSC using the constant reactive power design method and the proposed method.

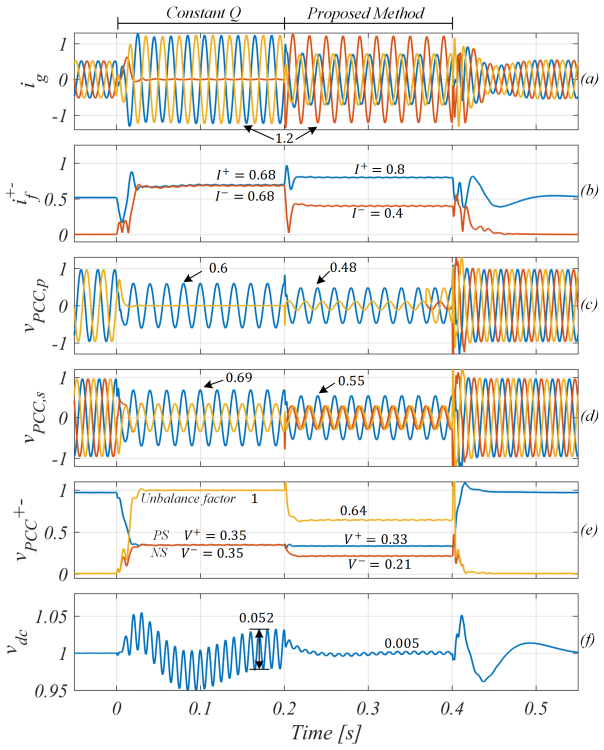

Fig. 13. Simulation results for a double line-to-ground solid fault for FPNSC using the constant reactive power design method and the proposed method.

difference between k_1 in the two strategies cannot be seen since $P^* = 0$. Apart from that, if one takes the positive and negative sequence voltage components of the PCC voltage from Fig. 10, then the value of k_2 for the proposed method and constant active power is almost identical, which explain their alike performance during this specific case.

C. Comparison to Constant Reactive Power Strategy

Finally, the results obtained using the constant reactive power strategy of FPNSC compared to the proposed method are displayed in Fig. 12, Fig. 13, and Fig. 14. It can be seen that the voltage unbalance factor and dc-link voltage ripple for all the three fault types are considerably improved with the proposed method as the injection of negative sequence inductive current is provided. Besides this, for the case of an SLG fault and a line-to-line fault, the proposed method eliminates the severe over-voltages that arise at the primary and secondary side of the Dy transformer when employing the constant reactive power method.

D. Mapping of Full Comparison

For a clear comparison between the strategies, the main outcome regarding voltage unbalanced factor and phase over-voltages from the results in Fig. 6 - Fig. 14 are shown in Table II. Here it can be seen, that the proposed use of the FPNSC method is the only method that does not result in phase over-voltages during any of the fault types analyzed. Furthermore, the voltage unbalance factor is highly improved using the proposed method. It should be noticed that since the grid faults considered are solid, the voltage sag is so deep that

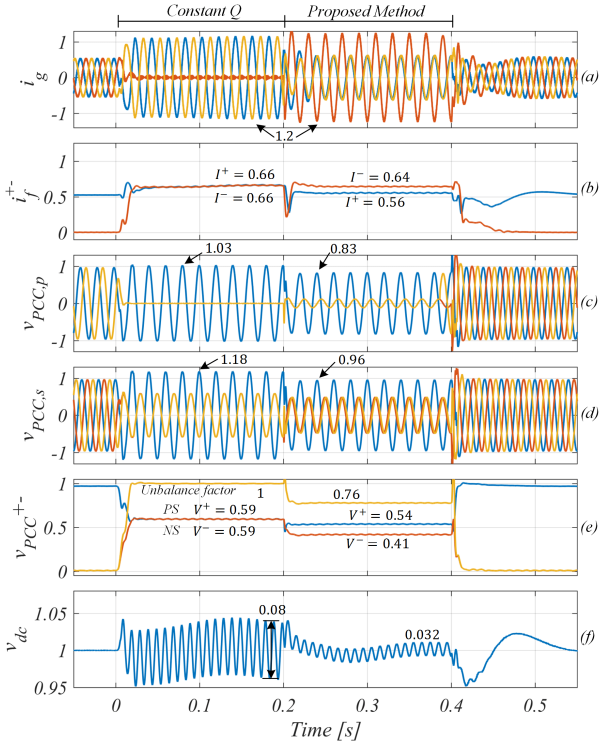

Fig. 14. Simulation results for a line-to-line solid fault for FPNSC using the constant reactive power design method and the proposed method.

TABLE II
COMPARISON BETWEEN THREE USAGES OF THE FPNSC METHOD AND THE PROPOSED DESIGN FOR THREE TYPES OF GRID FAULTS.

Fault Type	Metric	BPSC	Constant P	Constant Q	Proposed
Single Line-to-Ground	Voltage Unbalance Factor	0.61	0.55	0.68	**0.41**
Single Line-to-Ground	Phase over-voltage	**Yes (1.12)**	**Yes (1.01)**	**Yes (1.12)**	**No**
Double Line-to-Ground	Voltage Unbalance Factor	0.7	**0.63**	1	0.64
Double Line-to-Ground	Phase over-voltage	**No**	**No**	**No**	**No**
Line-to-Line	Voltage Unbalance Factor	0.87	0.82	1	**0.76**
Line-to-Line	Phase over-voltage	**Yes (1.13)**	**No**	**Yes (1.18)**	**No**
Compliance with recent grid codes		**No**	**No**	**No**	**Yes**

the method of constant active power injection will actually improve its performance in the sense of over-voltages and the voltage unbalance factor as the active power reference has to be reduced to zero during the fault to prioritize reactive power injection. Hence, as it has been shown, the proposed strategy complies with recently applicable and future grid codes in a flexible and general manner without exceeding the converter current limitation. To that end, the proposed strategy is shown to improve the performance of the fault ride-through of the converter in all cases when compared to the most conventional usage of the FPNSC strategy: BPSC, constant active power control, and constant reactive power control.

VI. Experimental Results

To verify the proposed method experimentally, a comparison to the BPSC is performed considering an SLG fault as well as a DLG fault. Compared to the simulated system, some modifications have been made for the laboratory setup. At first, a constant dc-link voltage is considered. Secondly, to be able to fully visualize the advantages of the proposed method, the coupling between the phase sequences, which occurs from the path between the faulted lines and the transformer grounding, needs to be included. However, this implies that a low impedance path must be physically constructed between the conducting phases and the grounding of the transformer. As this introduces very high short-circuit currents, this is not achievable in the laboratory due to limitations in the connected fault impedance and the power electronics-based grid simulator used to emulate the external grid. Due to this, the Dy transformer is neglected and the grid simulator is directly used to generate the asymmetrical voltage sag of interest. For a detailed description of the experimental setup used, please refer to [36]. The parameters listed in Table I is as well used for the experimental verification. The experimental results of the BPSC and the proposed method for an SLG fault and a DLG fault are presented in Fig. 15(a) and Fig. 15(b), respectively. As the dc-link voltage is constant, the active and reactive power are shown in subfigure (e) instead.

In this way, since oscillations in the active power are translated to the dc-link voltage, the active power can be seen as a verification of the dc-link voltages shown for the simulated cases in Fig. 6 and Fig. 7. Without the Dy transformer, it is seen that the exact values for the positive-sequence, negative-sequence, and VUF of the PCC voltage are different. However, the same trend is observed as the proposed method improves the VUF and decreases the peak value of the phase voltages, meaning that in a realistic scenario of an SLG fault, the over-voltage issue seen on the primary side of the transformer will be eliminated using the proposed method. The similar behavior is seen for the DLG in Fig. 15(b) where the sequence components are different but the VUF is again improved. Additionally, it can be observed that the active power is nearly constant during the DLG fault using the proposed method. This is in direct agreement with the simulation results presented in Fig. 7 where the dc-link voltage was observed to be nearly constant. Consequently, the presented experimental results of the modified experimental setup do indeed verify the performance and advantages of the proposed method.

VII. Conclusion

Addressing the recently enforced and next generation grid codes, this paper proposes a flexible and general control strategy for asymmetrical fault ride-through of grid-connected VSCs. A thorough derivation of the employed asymmetrical current reference strategy alongside an analytical expression for the maximum converter current are given. This, together with requirements from recent grid codes of asymmetrical current provision during unbalanced faults, is used to formulate an extension of the FPNSC method where the current reference generation is uniquely determined by the fault condition and predefined constants from the grid code. The proposed method is verified during three severe asymmetrical fault conditions: a single-line-to-ground fault, a double-line-to-ground fault, and a line-to-line fault, which is then compared with an existing industrial solution alongside other popular usages of the FPNSC method. The contributions of this paper are twofold. Firstly, the proposed method enables compliance with modern and future grid code requirements regarding asymmetrical fault ride-through using a flexible and general formulation. Secondly, the highly utilized FPNSC method, which previously did not comprise uniquely determined controller coefficients and power references, is extended to be uniquely described by taking into account the aforementioned new grid code requirements for asymmetrical reactive current provision.

Appendix

Proof. To derive (34), the task is to identify P^* and Q^* from (26) such that the phase currents are limited to $\hat{I}$. Using the trigonometric identify that $\cos(a+b) = \cos(a)\cos(b) -$

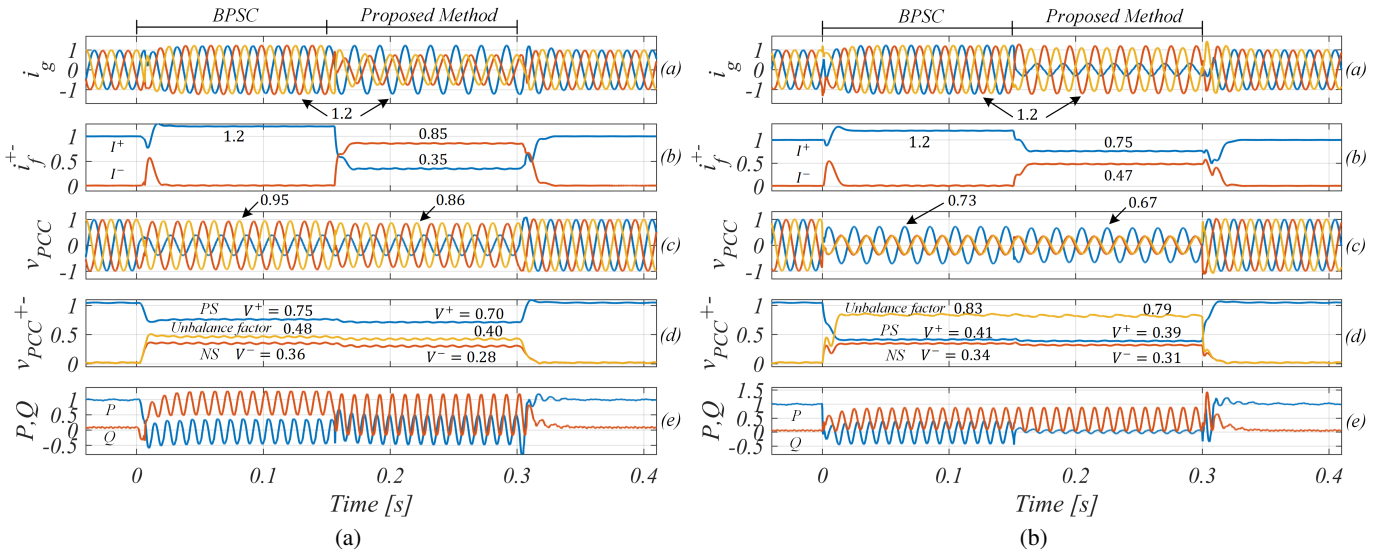

(a) (b)

Fig. 15. Experimental results for (a): an SLG solid fault and (b): a double line-to-ground solid fault for FPNSC using the BPSC design method and the proposed method.

$\sin(a)\sin(b)$, the term $2I^+I^-\cos(2\gamma+\delta-\theta_n-\theta_p)$ in (26) can be written as

$$2I^+I^-\left(\cos(2\gamma+\delta)\cos(\theta_p+\theta_n)+\sin(2\gamma+\delta)\sin(\theta_p+\theta_n)\right) \tag{41}$$

since cosine and sine are even and odd functions, respectively. By again using the trigonometric identity to expand $\cos(\theta_p+\theta_n)$ and $\sin(\theta_p+\theta_n)$, one can express (41) as

$$\begin{aligned}&2I^+I^-\cos(2\gamma+\delta)\left(\cos(\theta_p)\cos(\theta_n)-\sin(\theta_p)\sin(\theta_n)\right)\\&+2I^+I^-\sin(2\gamma+\delta)\left(\sin(\theta_p)\cos(\theta_n)+\cos(\theta_p)\sin(\theta_n)\right).\end{aligned} \tag{42}$$

Referring to the definitions from (18) and (19), then

$$\begin{aligned}I_p^+&=I^+\cos(\theta_p),\quad I_q^+=I^+\sin(\theta_p),\\I_p^-&=I^-\cos(\theta_n),\quad I_q^-=I^-\sin(\theta_n).\end{aligned}$$

Using these, (42) can be expressed as

$$2\cos(2\gamma+\delta)(I_p^+I_p^--I_q^+I_q^-)+2\sin(2\gamma+\delta)(I_q^+I_p^-+I_p^+I_p^-). \tag{43}$$

Finally, by inserting the definitions from (12)-(15), (18), (19) and (43) into

$$\hat{I}^2=(I^+)^2+(I^-)^2+2I^+I^-\cos(2\gamma+\delta-\theta_n-\theta_p) \tag{44}$$

and collecting the terms of P^* and Q^*, one arrives at the expression presented in (34). □

REFERENCES

[1] M. H. Bollen, *Understanding Power Quality Problems: Voltage Sags and Interruptions*. Wiley-IEEE Press, 1st ed., 1999.

[2] Ö. Göksu, R. Teodorescu, C. L. Bak, F. Iov, and P. C. Kjær, "Impact of wind power plant reactive current injection during asymmetrical grid faults," *IET Renewable Power Generation*, vol. 7, pp. 484–492, Sept 2013.

[3] T. Wijnhoven, G. Deconinck, T. Neumann, and I. Erlich, "Control aspects of the dynamic negative sequence current injection of type 4 wind turbines," in *Proc. IEEE PESGM*, pp. 1–5, July 2014.

[4] X. Du, Y. Wu, S. Gu, H. M. Tai, P. Sun, and Y. Ji, "Power oscillation analysis and control of three-phase grid-connected voltage source converters under unbalanced grid faults," *IET Power Electronics*, vol. 9, no. 11, pp. 2162–2173, 2016.

[5] M. Castilla, J. Miret, J. L. Sosa, J. Matas, and L. G. d. Vicuña, "Grid-fault control scheme for three-phase photovoltaic inverters with adjustable power quality characteristics," *IEEE Trans. Power Electron.*, vol. 25, pp. 2930–2940, Dec 2010.

[6] S. K. Chaudhary, R. Teodorescu, P. Rodriguez, P. C. Kjaer, and A. M. Gole, "Negative sequence current control in wind power plants with vsc-hvdc connection," *IEEE Trans. Sustain. Energy*, vol. 3, pp. 535–544, July 2012.

[7] S. Mortazavian, M. M. Shabestary, and Y. A. I. Mohamed, "Analysis and dynamic performance improvement of grid-connected voltage–source converters under unbalanced network conditions," *IEEE Trans. Power Electron.*, vol. 32, pp. 8134–8149, Oct 2017.

[8] A. Camacho, M. Castilla, J. Miret, A. Borrell, and L. G. de Vicuna, "Active and reactive power strategies with limitation for distributed generation inverters during unbalanced grid faults," *IEEE Trans. Ind. Electron.*, vol. 62, pp. 1515–1525, March 2015.

[9] A. Moawwad, M. S. E. Moursi, and W. Xiao, "A novel transient control strategy for vsc-hvdc connecting offshore wind power plant," *IEEE Trans. Sustain. Energy*, vol. 5, pp. 1056–1069, Oct 2014.

[10] J. Jia, G. Yang, and A. H. Nielsen, "Investigation of grid-connected voltage source converter performance under unbalanced faults," in *Proc. IEEE PES APPEEC*, pp. 609–613, Oct 2016.

[11] F. Wang, J. L. Duarte, and M. A. M. Hendrix, "Pliant active and reactive power control for grid-interactive converters under unbalanced voltage dips," *IEEE Trans. Power Electron.*, vol. 26, pp. 1511–1521, May 2011.

[12] S. Alepuz, S. Busquets-Monge, J. Bordonau, J. A. Martinez-Velasco, C. A. Silva, J. Pontt, and J. Rodriguez, "Control strategies based on symmetrical components for grid-connected converters under voltage dips," *IEEE Trans. Ind. Electron.*, vol. 56, pp. 2162–2173, June 2009.

[13] M. A. A. Rani, C. Nagamani, G. S. Ilango, and A. Karthikeyan, "An effective reference generation scheme for dfig with unbalanced grid voltage," *IEEE Trans. Sustain. Energy*, vol. 5, pp. 1010–1018, July 2014.

[14] P. Rodriguez, A. V. Timbus, R. Teodorescu, M. Liserre, and F. Blaabjerg, "Flexible active power control of distributed power generation systems during grid faults," *IEEE Trans. Ind. Electron.*, vol. 54, pp. 2583–2592, Oct 2007.

[15] P. Rodriguez, A. Timbus, R. Teodorescu, M. Liserre, and F. Blaabjerg, "Reactive power control for improving wind turbine system behavior under grid faults," *IEEE Trans. Power Electron.*, vol. 24, pp. 1798–1801, July 2009.

[16] J. Jia, G. Yang, and A. H. Nielsen, "A review on grid-connected converter control for short-circuit power provision under grid unbalanced faults," *IEEE Trans. Power Del.*, vol. 33, pp. 649–661, April 2018.

[17] A. Junyent-Ferre, O. Gomis-Bellmunt, T. C. Green, and D. E. Soto-Sanchez, "Current control reference calculation issues for the operation of renewable source grid interface vscs under unbalanced voltage sags," *IEEE Trans. Power Electron.*, vol. 26, pp. 3744–3753, Dec 2011.
[18] I. Erlich, T. Neumann, F. Shewarega, P. Schegner, and J. Meyer, "Wind turbine negative sequence current control and its effect on power system protection," in *Proc. IEEE PESGM*, pp. 1–5, July 2013.
[19] Ö. Göksu, N. A. Cutululis, P. Sørensen, and L. Zeni, "Asymmetrical fault analysis at the offshore network of hvdc connected wind power plants," in *IEEE Manchester PowerTech*, pp. 1–5, June 2017.
[20] S. Revelo and C. A. Silva, "Current reference strategy with explicit negative sequence component for voltage equalization contribution during asymmetric fault ride through," *International Transaction on Electrical Energy Systems*, vol. 25, pp. 3449–3471, December 2014.
[21] VDE, "VDE-AR-N 4120: Technical requirements for the connection and operation of customer installations to the high-voltage network (TCC high-voltage)," 2015.
[22] VDE, "VDE-AR-N 4110: Technical requirements for the connection and operation of customer installations to the medium-voltage network (TCC medium-voltage)," 2017.
[23] VDE, "Summary of the draft vde-ar-n 4110:2017-02." https://www.vde.com/resource/blob/1674522/46ee71927b557be9bd9fc7f59c2c70f7/summary-tar-ms-data.pdf, Feb. 2017. [Online; accessed 04-June-2019].
[24] VDE, "Summary of the draft vde-ar-n 4120:2017-05." https://www.vde.com/resource/blob/1667900/836e3781b72b3b726f509c90e35e339d/tar-hs-summaryen-data.pdf, May 2017. [Online; accessed 04-June-2019].
[25] M. A. G. López, J. L. G. de Vicuña, J. Miret, M. Castilla, and R. Guzmán, "Control strategy for grid-connected three-phase inverters during voltage sags to meet grid codes and to maximize power delivery capability," *IEEE Trans. Power Electron.*, vol. 33, pp. 9360–9374, Nov 2018.
[26] D. Shin, K. Lee, J. Lee, D. Yoo, and H. Kim, "Implementation of fault ride-through techniques of grid-connected inverter for distributed energy resources with adaptive low-pass notch pll," *IEEE Trans. Power Electron.*, vol. 30, pp. 2859–2871, May 2015.
[27] A. Camacho, M. Castilla, J. Miret, R. Guzman, and A. Borrell, "Reactive power control for distributed generation power plants to comply with voltage limits during grid faults," *IEEE Trans. Power Electron.*, vol. 29, pp. 6224–6234, Nov 2014.
[28] A. Camacho, M. Castilla, J. Miret, L. G. de Vicuña, and R. Guzman, "Positive and negative sequence control strategies to maximize the voltage support in resistive–inductive grids during grid faults," *IEEE Trans. Power Electron.*, vol. 33, pp. 5362–5373, June 2018.
[29] T. Neumann, T. Wijnhoven, G. Deconinck, and I. Erlich, "Enhanced dynamic voltage control of type 4 wind turbines during unbalanced grid faults," *IEEE Trans. Energy Conv.*, vol. 30, pp. 1650–1659, Dec 2015.
[30] M. M. Shabestary and Y. A. I. Mohamed, "Asymmetrical ride-through and grid support in converter-interfaced dg units under unbalanced conditions," *IEEE Trans. Ind. Electron.*, vol. 66, pp. 1130–1141, Feb 2019.
[31] P. Rodriguez, R. Teodorescu, I. Candela, A. V. Timbus, M. Liserre, and F. Blaabjerg, "New positive-sequence voltage detector for grid synchronization of power converters under faulty grid conditions," in *37th IEEE Power Electronics Specialists Conference*, pp. 1–7, June 2006.
[32] P. Rodriguez, J. Pou, J. Bergas, J. I. Candela, R. P. Burgos, and D. Boroyevich, "Decoupled double synchronous reference frame pll for power converters control," *IEEE Trans. Power Electron.*, vol. 22, pp. 584–592, March 2007.
[33] M. M. Shabestary and Y. A. I. Mohamed, "An analytical method to obtain maximum allowable grid support by using grid-connected converters," *IEEE Trans. Sustain. Energy*, vol. 7, pp. 1558–1571, Oct 2016.
[34] E. Behrouzian and M. Bongiorno, "Investigation of negative-sequence injection capability of cascaded h-bridge converters in star and delta configuration," *IEEE Trans. Power Electron.*, vol. 32, pp. 1675–1683, Feb 2017.
[35] I. M. Sanz, P. D. Judge, C. E. Spallarossa, B. Chaudhuri, and T. C. Green, "Dynamic overload capability of vsc hvdc interconnections for frequency support," *IEEE Trans. Energy Conv.*, vol. 32, pp. 1544–1553, Dec 2017.
[36] M. G. Taul, X. Wang, P. Davari, and F. Blaabjerg, "An overview of assessment methods for synchronization stability of grid-connected converters under severe symmetrical grid faults," *IEEE Trans. Power Electron.*, pp. 1–1, 2019.

Mads Graungaard Taul (S'17) received the B.Sc. and M.Sc. degree in Energy Technology with specializing in Electrical Energy Engineering and Power Electronics and Drives from Aalborg University, Denmark in 2016 and 2019, respectively. Currently, he is pursuing a Ph.D. in Power Electronic Systems with the Department of Energy Technology at Aalborg University, Denmark. His main research interests include renewable energy sources and grid-connected converters with a special focus on modeling and control of power electronic-based power systems under grid fault conditions.

Xiongfei Wang (S'10-M'13-SM'17) received the B.S. degree from Yanshan University, Qinhuangdao, China, in 2006, the M.S. degree from Harbin Institute of Technology, Harbin, China, in 2008, both in electrical engineering, and the Ph.D. degree in energy technology from Aalborg University, Aalborg, Denmark, in 2013. Since 2009, he has been with the Department of Energy Technology, Aalborg University, where he became Assistant Professor in 2014, an Associate Professor in 2016, a Full Professor and Research Program Leader for Electronic Power Grid Infrastructure in 2018. His current research interests include modeling and control of grid-interactive power converters, stability and power quality of power electronic based power systems, active and passive filters. Dr. Wang serves as an Associate Editor for the IEEE TRANSACTIONS ON POWER ELECTRONICS, the IEEE TRANSACTIONS ON INDUSTRY APPLICATIONS, and the IEEE JOURNAL OF EMERGING AND SELECTED TOPICS IN POWER ELECTRONICS. He was selected into Aalborg University Strategic Talent Management Program in 2016. He received six IEEE prize paper awards, the outstanding reviewer award of IEEE TRANSACTIONS ON POWER ELECTRONICS in 2017, and the IEEE PELS Richard M. Bass Outstanding Young Power Electronics Engineer Award in 2018.

Pooya Davari (S'11–M'13) received the B.Sc. and M.Sc. degrees in electronic engineering from the University of Mazandaran, Babolsar, Iran, in 2004 and 2008, respectively, and the Ph.D. degree in power electronics from Queensland University of Technology (QUT), Brisbane, Australia, in 2013. From 2005 to 2010, he was involved in several electronics and power electronics projects as a Development Engineer. From 2010 to 2014, he investigated and developed high-power high-voltage power electronic systems for multidisciplinary projects, such as ultrasound application, exhaust gas emission reduction, and tissue-materials sterilization. From 2013 to 2014, he was a Lecturer with QUT. He joined as a Postdoctoral Researcher the Department of Energy Technology, Aalborg University, Aalborg, Denmark, in 2014, where he is currently an Associate Professor. His current research interests include EMI/EMC in power electronics, WBG-based power converters, active front-end rectifiers, harmonic mitigation in adjustable-speed drives, and pulsed power applications. Dr. Davari received a research grant from the Danish Council of Independent Research in 2016.

Frede Blaabjerg (S'86–M'88–SM'97–F'03) was with ABB-Scandia, Randers, Denmark, from 1987 to 1988. From 1988 to 1992, he got the PhD degree in Electrical Engineering at Aalborg University in 1995. He became an Assistant Professor in 1992, an Associate Professor in 1996, and a Full Professor of power electronics and drives in 1998. From 2017 he became a Villum Investigator. He is honoris causa at University Politehnica Timisoara (UPT), Romania and Tallinn Technical University (TTU) in Estonia. His current research interests include power electronics and its applications such as in wind turbines, PV systems, reliability, harmonics and adjustable speed drives. He has published more than 600 journal papers in the fields of power electronics and its applications. He is the co-author of four monographs and editor of ten books in power electronics and its applications. He has received 30 IEEE Prize Paper Awards, the IEEE PELS Distinguished Service Award in 2009, the EPE-PEMC Council Award in 2010, the IEEE William E. Newell Power Electronics Award 2014 and the Villum Kann Rasmussen Research Award 2014. He was the Editor-in-Chief of the IEEE TRANSACTIONS ON POWER ELECTRONICS from 2006 to 2012. He has been Distinguished Lecturer for the IEEE Power Electronics Society from 2005 to 2007 and for the IEEE Industry Applications Society from 2010 to 2011 as well as 2017 to 2018. In 2019-2020 he serves a President of IEEE Power Electronics Society. He is Vice-President of the Danish Academy of Technical Sciences too. He is nominated in 2014-2018 by Thomson Reuters to be between the most 250 cited researchers in Engineering in the world.